



Article

Homogeneous Incorporation of Gallium into Layered Double Hydroxide Lattice for Potential Radiodiagnostics: Proof-of-Concept

Do-Gak Jeung ¹, Tae-Hyun Kim ^{2,*} and Jae-Min Oh ^{1,*}

¹ Department of Energy and Materials Engineering, Dongguk University-Seoul, Seoul 04620, Korea; jdk941101@naver.com

² Department of Environmental Engineering, Seoul National University of Science and Technology, Seoul 01811, Korea

* Correspondence: th.kim@seoultech.ac.kr (T.-H.K.); jaemin.oh@dongguk.edu (J.-M.O.)

Abstract: Trivalent gallium ion was successfully incorporated into chemically well-defined MgAl-layered double hydroxide (LDH) frameworks through postsynthetic hydrothermal treatment. Quantitative analysis with inductively coupled plasma-mass spectroscopy exhibited that Ga³⁺ was first incorporated into LDH through partial dissolution-precipitation at the edge of LDH particle and homogeneously distributed throughout the particle by substitution of Ga³⁺ for Al³⁺ in LDH frameworks. The powder X-ray diffraction patterns showed that the Ga³⁺ incorporation did not affect the crystal structure without evolution of unexpected impurities. The morphology and surface property of LDH evaluated by scanning electron microscopy and light scattering showed the preservation of physicochemical properties throughout 24 h of hydrothermal reaction. The distribution of incorporated Ga³⁺ was visualized with energy dispersive spectroscopy-assisted transmission electron microscopy, suggesting the homogeneous location of Ga³⁺ in an LDH particle. The X-ray absorption near-edge structure and extended X-ray absorption fine structure suggested that the Ga moiety was immobilized in LDH from 0.5 h and readily crystallized upon reaction time.

Keywords: layered double hydroxide; hydrothermal treatment; gallium; incorporation; diagnostics



Citation: Jeung, D.-G.; Kim, T.-H.; Oh, J.-M. Homogeneous Incorporation of Gallium into Layered Double Hydroxide Lattice for Potential Radiodiagnostics: Proof-of-Concept. *Nanomaterials* **2021**, *11*, 44. <https://dx.doi.org/10.3390/nano11010044>

Received: 27 November 2020

Accepted: 24 December 2020

Published: 26 December 2020

Publisher's Note: MDPI stays neutral with regard to jurisdictional claims in published maps and institutional affiliations.



Copyright: © 2020 by the authors. Licensee MDPI, Basel, Switzerland. This article is an open access article distributed under the terms and conditions of the Creative Commons Attribution (CC BY) license (<https://creativecommons.org/licenses/by/4.0/>).

1. Introduction

For decades, layered double hydroxide (LDH) has attracted enormous interest as drug delivery carrier [1,2]. The LDH is composed of positively charged mixed metal hydroxide layers and charge compensating interlayer anions, with general chemical formula of M(II)_{1-x}M(III)_x(OH)₂(Aⁿ⁻)_{x/n} mH₂O, where M²⁺, M³⁺, and Aⁿ⁻ represented divalent, trivalent metal cations, and interlayer anion, respectively [3,4]. Due to the diverse metal composition and pH dependent solubility, LDH has been known to show high biocompatibility and biological inertness [5,6]. The unique properties of LDH such as anion exchange capacity, high cellular uptake, and controlled release of interlayer anion, allowed LDH to exhibit great potential as delivery carrier [7–9]. There have been extensive studies to encapsulate, stabilize, and deliver bioactive moieties such as anticancer drug [10], natural extract [11], antibiotics [2], nucleic acid [7], etc. utilizing LDH as a platform. In order to not only comprehend biological behavior of LDH carriers but also take advantage of diagnosis, many researchers have tried to incorporate tracing moieties into LDH for imaging [12]. Fluorescent dyes are one of the widely used labeling agents in laboratory level for in vitro and in vivo research due to high accessibility [13,14]. Recently, LDHs labeled with contrasting moieties, such as gadolinium (Gd) complex [15,16] and metallic nanoparticles [17] for magnetic resonance imaging (MRI) and X-ray computed tomography (CT), respectively, have been developed. However, those tracing moieties were bound to the external surface of LDH [17] or intercalated electrostatically between LDH layers [15,18], giving rise to

stability issue of tracing agent under systemic circumstances. To address this stability issue, robust labeling such as direct incorporation of tracing moiety into the lattice of LDH has been arisen recently [19,20].

Among various labeling agent, radioisotope (RI) has emerged as a powerful tracer due to great sensitivity, outstanding tissue penetration, possible quantification, and excellent translation potential [21–25]. Currently, RI-based imaging such as single-photon emission computed tomography (SPECT) and positron emission tomography (PET) show high clinical accessibility. Taking into account the advantage of RI in imaging and delivery functionality of LDH, the incorporation of RI, e.g., ^{57}Co or ^{67}Ga into LDH frameworks became an option for diagnostic application [26–28].

However, direct incorporation of radionuclides into the LDH lattice for potential application in biological imaging is challenging. In order to take the maximum advantages of LDH in biological system, well-defined crystalline phase and uniform particle size are important factors [8,29,30]. Although LDH phase is easily formed within an hour through coprecipitating metal cations, thus prepared LDH used to have impurity and size problems. Fairly high content (~30%) of amorphous aluminum hydroxide, which is not detected by X-ray diffraction, was observed in the MgAl-LDH prepared by coprecipitation [31]. Unal et al. reported that preparation of MgGa-LDH without impurity—GaOOH or Ga₂O₃—requires high temperature (~200 °C) and long reaction time [32]. Furthermore, the coprecipitated LDH at short time produces small particles, which tends to form large aggregates [33,34]. In order to address the purity and particle size, LDH aimed for biological application is often prepared through hydrothermal reaction [35]. However, preparation of pure and particle size controlled LDH through hydrothermal reaction requires longer time, and thus, it is not a recommended method to incorporate radionuclide with short half-life (e.g., $t_{1/2}$ of ^{68}Ga and ^{44}Sc are 68 min and 3.97 h, respectively) [36,37] into LDH. To overcome this time mismatch, Kim et al. reported direct incorporation of divalent ^{57}Co , a single-photon emission computed tomography (SPECT)-sensitive RI, into the crystal lattice of LDH through hydrothermal substitution, which preserved morphology and crystallinity of LDH during short incorporation time [27,28]. Sufficient radiolabeling and tumor targeting efficacy were also addressed with the reported method, presenting the potential of LDH as radiodiagnosis.

This research might expand this concept to trivalent metal like gallium (Ga^{3+}). As ^{68}Ga is well known as PET imaging agent, the incorporation of gallium into LDH would suggest an alternative in contrasting agent. As a proof-of-concept experiment, this research proposed methodology to introduce nonradioactive Ga^{3+} into the LDH lattice preserving physicochemical properties. Through previous researches, incorporation methodology for certain metal species into layered metal hydroxide lattice, such as LDH [38] or brucite ($\text{Mg}(\text{OH})_2$) [39], was investigated. Divalent cation Co^{2+} was successfully incorporated into MgAl-LDH lattice through hydrothermal treatment-assisted isomorphous substitution for Mg^{2+} in the LDH lattice [38]. Furthermore, the Al^{3+} cations could be incorporated into $\text{Mg}(\text{OH})_2$ through partial dissolution-reprecipitation accompanying phase transformation from brucite to LDH [39]. Both cases showed successful introduction of target cations while preserving crystallinity and particle size. However, stabilized incorporation of $\text{Ga}^{3+}(\text{aq})$ into LDH lattice at short time with preserved crystalline phase and particle size is another challenging project. Due to the strong acidity, the LDH is spontaneously dissolved upon encountering $\text{Ga}^{3+}(\text{aq})$, resulting in full dissolution-reprecipitation rather than incorporation of metal. In order to solve the problem, in this research, pretreated $\text{Ga}^{3+}(\text{aq})$ with NaOH to get $\text{Ga}(\text{OH})_4^-$ species, which would react with LDH for incorporation, was utilized. Referring to the previous metal substitution method [27], $\text{Ga}(\text{OH})_4^-$ and presynthesized LDH were reacted under hydrothermal condition. From this methodology, fast Ga^{3+} incorporation into LDH lattice were expected while preserving physicochemical properties of parent LDH such as morphology, surface charge, and crystallinity. To comprehend the detailed incorporation process of Ga^{3+} cation, time-dependent characterizations such as X-ray diffraction (XRD), field-emission scanning electron microscopy (FE-SEM), dynamic

light scattering (DLS), electrophoretic light scattering, inductively coupled plasma-mass spectrometer (ICP-MS), energy dispersive spectroscopy-assisted transmission electron microscopy (TEM-EDS) mapping, and X-ray absorption spectroscopy (XAS) on designed time points (0.5, 1, 2, 3, 6, 12, and 24 h) were carried out. In the result and discussion section, this research will propose the incorporation mechanism first and demonstrate each aspect with corresponding characterization.

2. Materials and Methods

2.1. Materials

Magnesium nitrate hexahydrate ($\text{Mg}(\text{NO}_3)_2 \cdot 6\text{H}_2\text{O}$), aluminum nitrate nonahydrate ($\text{Al}(\text{NO}_3)_3 \cdot 9\text{H}_2\text{O}$), and gallium nitrate hydrate ($\text{Ga}(\text{NO}_3)_3 \cdot x\text{H}_2\text{O}$) were obtained from Sigma-Aldrich Co. LLC. (St. Louis, MO, USA). Sodium hydroxide pellet (NaOH) and sodium hydrogencarbonate (NaHCO_3) were acquired from Daejung Chemicals & Metals Co. Ltd. (Siheung-si, Gyeonggi-do, Korea). All reagents were utilized without further purification.

2.2. Synthesis of Parent MgAl-LDH

The parent MgAl-LDH with well-controlled particle size was synthesized by conventional coprecipitation and consecutive hydrothermal treatment. The mixed metal solution of $\text{Mg}(\text{NO}_3)_2 \cdot 6\text{H}_2\text{O}$ (0.315 M) and $\text{Al}(\text{NO}_3)_3 \cdot 9\text{H}_2\text{O}$ (0.105 M) was titrated with mixed alkaline solution of NaOH (1.2 M)/ NaHCO_3 (0.126 M) until pH 9.5. The obtained slurry was transferred to a Teflon-lined stainless-steel bomb and then reacted at 150 °C for 24 h. After then, precipitate was centrifuged, washed with deionized water, and lyophilized. The obtained parent MgAl- CO_3 -LDH powder was directly utilized for Ga^{3+} substitution through hydrothermal reaction.

2.3. Incorporation of Ga^{3+} into LDH

An aqueous suspension containing MgAl-LDH (5 mg/mL) and $\text{Ga}(\text{NO}_3)_3 \cdot x\text{H}_2\text{O}$ solution (0.05 M) was prepared separately. The $\text{Ga}(\text{NO}_3)_3 \cdot x\text{H}_2\text{O}$ solution was titrated by NaOH solution until pH 12 to produce $\text{Ga}(\text{OH})_4^-$ as reactant. Then, LDH suspension was added to titrated $\text{Ga}(\text{NO}_3)_3 \cdot x\text{H}_2\text{O}$ solution and the mixture was hydrothermally treated in Teflon-lined stainless steel bomb at 150 °C. At each designed time points, 0.5, 1, 2, 3, 6, 12, and 24 h, the reaction was quenched and solid part was centrifuged, washed, and lyophilized. The Ga^{3+} incorporated LDH were represented as Ga@LDH-n , where n stands for the reaction time in hours.

2.4. Characterization

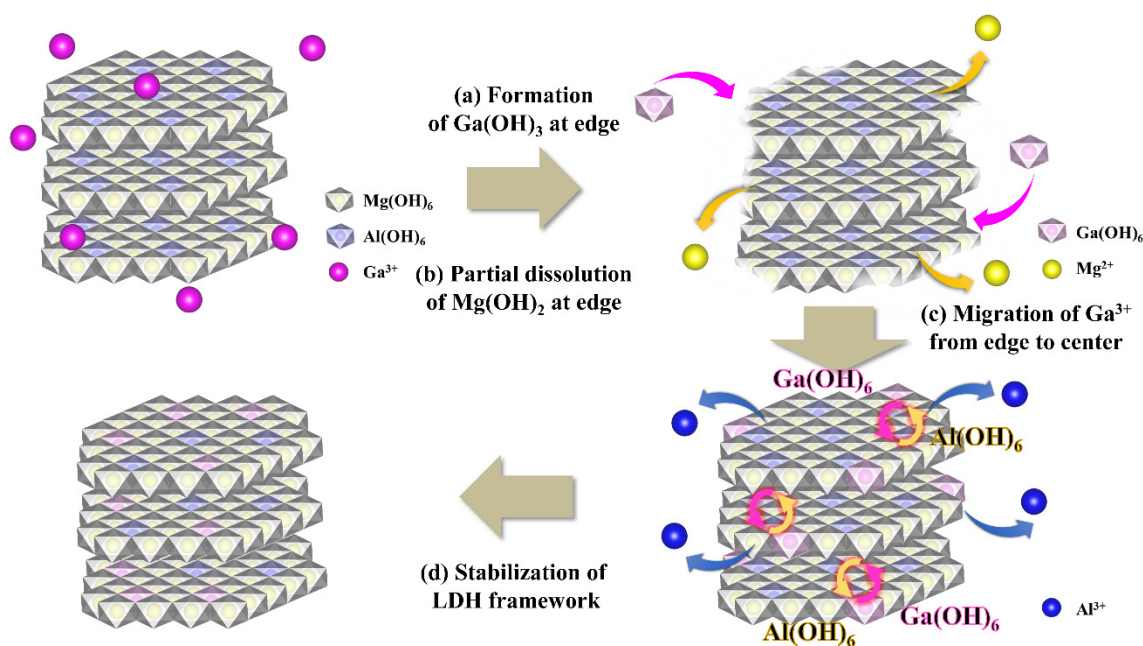
The XRD patterns of parent LDH and Ga@LDHs were obtained by X-ray diffractometer (SmartLab, Rigaku, Tokyo, Japan) with $\text{Cu K}\alpha$ radiation ($\lambda = 1.5406 \text{ \AA}$) in the 2θ range of 5° – 70° with scanning rate of $0.05^\circ/\text{s}$. Lattice parameters were calculated with UnitCell software (Tim Holland & Simon Redfern, 2006, Cambridge University, England) based on the obtained diffractograms. The crystallite sizes along the *c*-axis and *ab*-plane were calculated by Scherrer's equation ($t = 0.9\lambda/B\cos\theta$, *t*: crystallite size (Å), λ : X-ray wavelength, *B*: full-width at half-maximum of peak, θ : Bragg angle) [40] utilizing (003) and (110) peak, respectively. The contents of Ga^{3+} in Ga@LDHs were obtained by inductively coupled plasma-mass spectrometer (ICP-MS, NexION 2000, PerkinElmer, Middlesex, MA, USA). Hydrodynamic radii and zeta potential values of samples were examined by ELSZ-1000 (Otsuka, Kyoto, Japan) at 1 mg/mL concentration. The particle size and surface morphology of parent LDH, and Ga@LDHs were observed using field emission-scanning electron microscope (FE-SEM, JSM-7100F, JEOL, Tokyo, Japan). For SEM measurement, powdered samples were directly attached on carbon tape and then images were obtained with 15 kV acceleration voltage after Pt sputtering for 60 s. To obtain the average particle size and sample thickness, 50 particles were randomly selected from SEM images. In order to visualize the distribution of metal ions in Ga@LDHs, field-emission transmission electron

microscopy (FE-TEM) and energy dispersive spectroscopy (EDS) mapping were performed (FE-TEM, Titan G2 ChemiSTEM Cs Probe, FEI, Hillsboro, OR, USA). To prepare TEM specimen, each powdered sample was dispersed into deionized water with ultrasonication for 10 min, and a drop of suspension was placed on 200-square mesh copper grid with carbon film. The TEM and EDS mapping images were acquired utilizing 200 kV accelerated electron beam. The local chemical environment around the incorporated Ga atoms was analyzed by X-ray absorption spectroscopy (XAS) at 8C NanoXAFS beamline in the Pohang Accelerator Laboratory (PAL), Pohang, Korea. All the powder-type samples were measured in transmission mode at Ga K-edge (10,375 eV). Normalized X-ray absorption near-edge structure (XANES) and extended X-ray absorption fine structure (EXAFS) spectra were obtained using Athena software.

3. Result and Discussion

3.1. Proposed Incorporation Mechanism of Ga^{3+} into LDH

Inspired by the previous substitution researches on LDH and brucite ($\text{Mg}(\text{OH})_2$) [38,39] and study on anion exchange from MgAl-CO_3 to MgAl-NO_3 under acidic condition [41], the Ga^{3+} incorporation mechanism were hypothesized that homogeneous incorporation of Ga^{3+} into the lattice of LDH would occur through following processes: (i) partial dissolution of LDH at the periphery, (ii) formation of amorphous $\text{Ga}(\text{OH})_3$ at the edge of LDH, (iii) migration of Ga^{3+} from the edge of LDH to the center by replacing Al^{3+} , (iv) stabilization of LDH framework with balanced M(II)/M(III) ratio (Scheme 1).



Scheme 1. Proposed mechanism of time-dependent Ga^{3+} incorporation reaction.

First of all, $\text{Ga}(\text{OH})_4^-$ anions approach the edge of LDH. As the solubility product (K_{sp}) of $\text{Ga}(\text{OH})_3$ (7.28×10^{-36}) is much lower than that of $\text{Mg}(\text{OH})_2$ (1.8×10^{-11}) but fairly comparable with that of $\text{Al}(\text{OH})_3$ (1.99×10^{-33}), the $\text{Ga}(\text{OH})_4^-$ ion could precipitate at the edge of LDH (Scheme 1 (a)) by partially dissolving $\text{Mg}(\text{OH})_2$ moiety (Scheme 1 (b)). In this process, equilibrium of Equation (1) lies to the right. The precipitation of $\text{Ga}(\text{OH})_3$ and dissolution of $\text{Mg}(\text{OH})_2$ would be soon stabilized through dynamic equilibrium of Equation (2), developing thin layer of $\text{Ga}(\text{OH})_3$ at the edge of LDH particle.



Then the outermost Ga^{3+} is expected to migrate from the edge to the center of LDH particle through solid solution process [39,42] (Scheme 1 (c)), as we previously observed in Al^{3+} incorporation into brucite layers [39]. This process is mediated by substitution of Ga^{3+} for Al^{3+} to balance M(II)/M(III) ratio of which value 2.0~3.5 is reported to thermodynamically stable LDH structure [43]. The replacement of Al^{3+} by Ga^{3+} is rationalized by the ionic radii: 76 pm for Ga^{3+} , 67.5 pm for Al^{3+} , and 86 pm for Mg^{2+} . The comparable ionic radius of Ga^{3+} to Mg^{2+} would facilitate the stabilization of Ga^{3+} instead of Al^{3+} in the LDH lattice. The released Al^{3+} is considered to exist as solubilized ion as the basic reaction pH favors $\text{Al}(\text{OH})_4^-$ species over $\text{Al}(\text{OH})_3$ precipitate.

3.2. Quantification of Metal Contents in Ga@LDHs

The chemical formulae of parent MgAl-LDH and Ga@LDHs (Table 1) supported the Ga^{3+} incorporation into LDH by replacing Al^{3+} . The amount of Ga^{3+} compared with Al^{3+} in Ga@LDHs increased with respect to reaction time, suggesting the continuous incorporation of Ga^{3+} . For quantitative analysis, time-dependent molar fraction of Ga^{3+} and Al^{3+} in Ga@LDHs was monitored based on the calculated chemical formulae (Figure 1A). The molar fraction of metal was defined by the ratio of certain metal over total metal content. The molar fraction of Ga^{3+} gradually increased from 0% to 2.6% along the reaction time (black line in Figure 1A), while the amount of Al^{3+} slightly increased from 20.3 to 21.8 but readily dropped to 19.8 (red dotted line in Figure 1A), showing continuous entering of Ga^{3+} into LDH by replacing Al^{3+} (Scheme 1 (c)). According to the increasing amount of Ga^{3+} , the molar ratio of pre-existing metals (Mg^{2+} and Al^{3+}) over supplied metal (Ga^{3+}) dramatically decreased by 10.5 times (from 379.7 at 0.5 h to 36.5 at 24 h) (black line in Figure 1B), suggesting continuous supply of Ga^{3+} into LDH (Scheme 1 (b)). Interestingly, the metal ratio between divalent metal (Mg^{2+}) and trivalent ones (Al^{3+} and Ga^{3+}) in final Ga@LDH was equilibrated after abrupt decrease by ~11.5% at early time point (1 h) (red dotted line in Figure 1B). This may be attributed to the dissolution of $\text{Mg}(\text{OH})_2$ at the edge in early stage and thermodynamic stabilization through metal ratio balancing [43]. Under hydrothermal condition, the outermost low crystalline $\text{Ga}(\text{OH})_3$ could diffuse into the main framework of LDH by replacing Al^{3+} as often found in solid-solution process [44,45], resulting in the stabilization of M(II):M(III) ratio. From these quantitative analyses, we could find that hydrothermal treatment enabled incorporation of Ga^{3+} into LDH within 0.5 h and the homogeneous distribution followed along with lattice rearrangement occurred during 24 h.

Table 1. Chemical formula, lattice parameters and calculated crystallite sizes of parent MgAl-layered double hydroxide (LDH) and Ga@LDH-n (where n stands for the reaction time in hours).

Sample	Chemical Formulae ^a	Lattice Parameter ^b (Å)		Crystallite Size ^c (nm)	
		a	c	(003)	(110)
MgAl-LDH	$\text{Mg}_{3.92}\text{Al}(\text{OH})_{9.84}(\text{CO}_3)_{0.5}$	3.06	24.37	25	31
Ga@LDH-0.5	$\text{Mg}_{3.86}\text{AlGa}_{0.01}(\text{OH})_{9.72}(\text{CO}_3)_{0.5}$	3.07	23.51	25	24
Ga@LDH-1	$\text{Mg}_{3.60}\text{AlGa}_{0.02}(\text{OH})_{9.20}(\text{CO}_3)_{0.5}$	3.07	23.58	24	23
Ga@LDH-2	$\text{Mg}_{3.56}\text{AlGa}_{0.03}(\text{OH})_{9.12}(\text{CO}_3)_{0.5}$	3.07	23.53	23	18
Ga@LDH-3	$\text{Mg}_{3.74}\text{AlGa}_{0.04}(\text{OH})_{9.48}(\text{CO}_3)_{0.5}$	3.07	23.55	28	27
Ga@LDH-6	$\text{Mg}_{3.81}\text{AlGa}_{0.07}(\text{OH})_{9.62}(\text{CO}_3)_{0.5}$	3.07	23.36	31	22
Ga@LDH-12	$\text{Mg}_{3.76}\text{AlGa}_{0.09}(\text{OH})_{9.52}(\text{CO}_3)_{0.5}$	3.07	23.38	40	25
Ga@LDH-24	$\text{Mg}_{3.92}\text{AlGa}_{0.13}(\text{OH})_{9.84}(\text{CO}_3)_{0.5}$	3.07	23.54	37	28

^a Quantified by inductively coupled plasma optical emission spectroscopy; ^b calculated with UnitCell software (Tim Holland & Simon Redfern, 2006, Cambridge University, England); ^c calculated by Scherrer's equation.

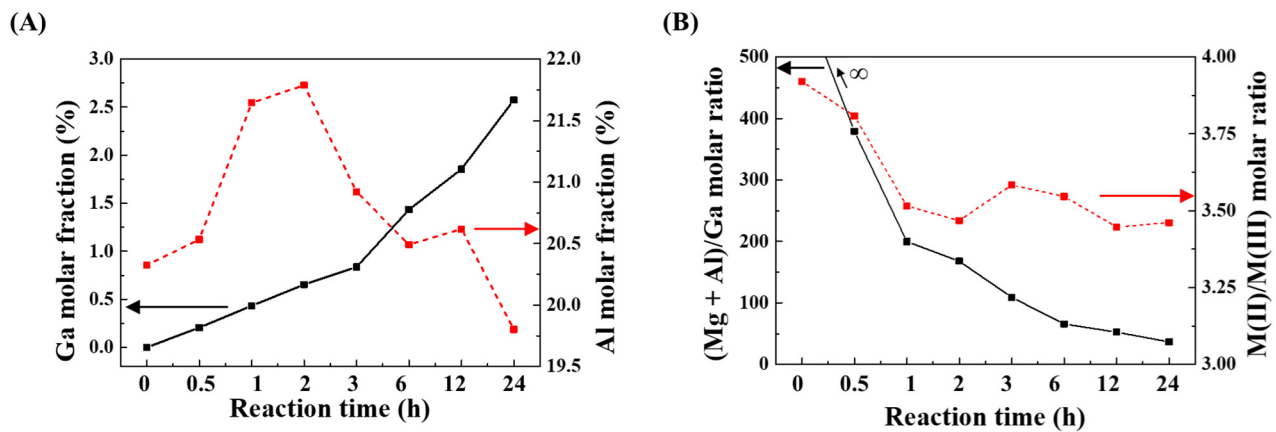


Figure 1. Quantitative result of (A) time-dependent molar fraction of Ga (black solid line, left y -axis) and Al (red dotted line, right y -axis) in Ga@LDHs. (B) Time-dependent (Mg + Al)/Ga ratio (black solid line, left y -axis) and M(II)/M(III) ratio (red dotted line) in Ga@LDHs by inductively coupled plasma-mass spectrometer (ICP-MS).

3.3. Crystal Structure and Crystalline Impurities Analysis

It is generally known that Ga^{3+} tends to develop thermodynamically stable gallium oxide hydroxide (GaOOH) under hydroxide-rich condition [40]. In order to exclude the formation of unexpected Ga and Al-impurity during incorporation reaction, the PXRD patterns of samples at representative time points were recorded (Figure 2). The diffractogram showed that parent MgAl-LDH had typical hydroxalcalite-like structure (JCPDS No. 14-0191) with sharp diffractions corresponding to (003) and (006) attributed to ordered 2-dimensional layer stacking [41]. In addition, the (110) and (113) diffraction from crystallographic ab -plane of LDH lattice were clearly observed at 60.4° and 61.7° , respectively.

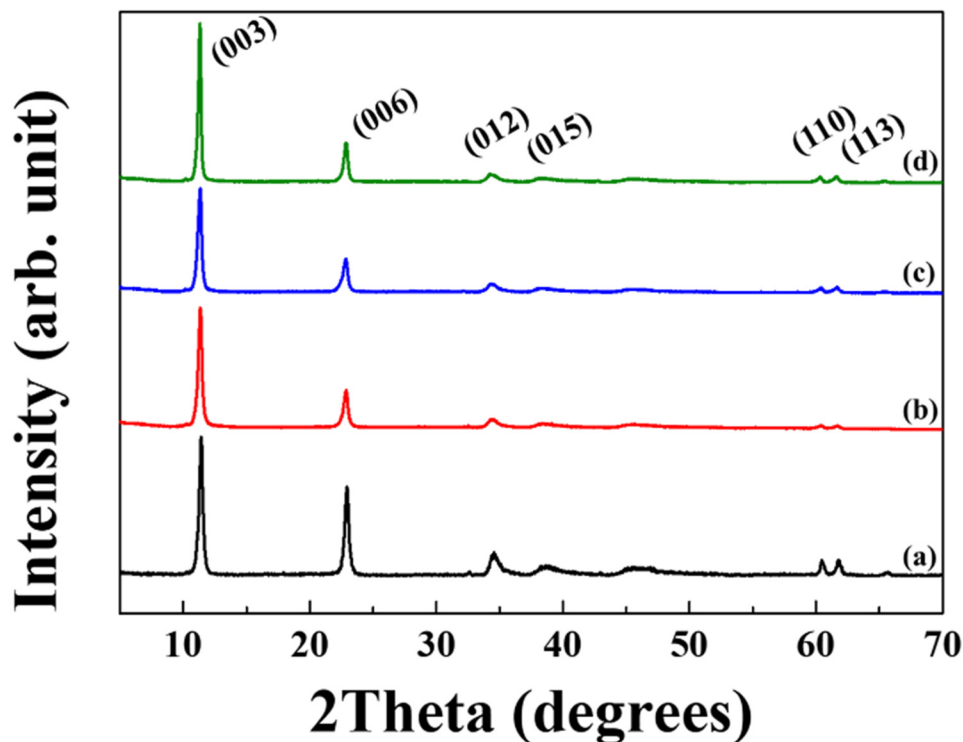


Figure 2. Powder X-ray diffraction patterns of (a) parent MgAl-layered double hydroxide (LDH), (b) Ga@LDH-0.5 (c) Ga@LDH-2, and (d) Ga@LDH-24.

The intensity of (003) reflection decreased along the reaction time until 3 h (Figure S1), which supported the partial dissolution of MgAl-LDH at early time point. After 3 h, the intensity of (003) diffraction gradually recovered upon homogeneous incorporation of Ga³⁺ in LDH structure. On the other hand, the reflections corresponding to *ab*-plane ((110) and (113)) apparently decreased. It is due to the evolution of partial dissolution of Al³⁺ during the substitution reaction [46]. Furthermore, XRD patterns of Ga@LDH shows only diffractions attributed by hydrocalcite without any possible impurities from Ga³⁺ and Al³⁺. It should be noted here that the lattice parameters of Ga@LDHs did not change significantly compared with parent MgAl-LDH (Table 1), suggesting that the global crystalline phase of LDH was not affected by the Ga³⁺ incorporation. To investigate the effect of reaction time on crystal structure in detail, the crystallite sizes along (003) and (110) direction were calculated by Scherrer's equation. The crystallite sizes decreased around 6% and 41% for (003) and (110), respectively, during 2 h, suggesting the partial dissolution of early stage (Scheme 1 (b)). The crystallite size along *c*-axis recovered from 3 h and increased approximately 45% after 24 h due to the facilitated layer stacking under hydrothermal condition. On the other hand, the crystallite size of *ab*-plane only recovered 88% of parent LDH after 24 h, implying the possible development of defect in the lattice by Ga³⁺ incorporation. From the XRD analysis, it was found that post hydrothermal treatment for Ga³⁺ incorporation did not affect to the crystal structure of parent LDH and replacing Al³⁺ ions did not form any impurities and were removed by washing process.

3.4. Morphology and Surface Properties

Morphology is one of the most important parameters of LDH for various applications especially biomedical fields. The electron microscopic images of parent MgAl-LDH showed plate-like particles with uniform lateral size (Figure 3), which was the characteristic feature of hydrothermally prepared LDHs [33]. The characteristic plate-like morphology of LDH was well preserved throughout the 24 h of Ga³⁺ incorporation reaction (Figure 3c–h and Figure S2) without any irregular particles assuming Ga or Al impurities. The average lateral size of parent LDH determined was ~142 nm; taking into account the average value and standard deviation (Table 2), the lateral dimension of Ga@LDH did not significantly change regardless of reaction time. This result exhibited that the slight reduction in crystallite size along *ab*-plane was attributed not to the particle shrinkage but to the reduced intracrystalline arrangement, as discussed in Section 3.3. On the other hand, the thickness of Ga@LDH dramatically increased from 19 to 42 nm after 24 h of reaction time, along with crystallite size increase through *c*-axis (Table 1). From the TEM images, we also confirmed that parent MgAl-LDH and Ga@LDHs had platelets in the range of 100–200 nm without serious changes corresponded to SEM images.

The hydrodynamic radii of Ga@LDHs in aqueous suspensions were monitored by dynamic light scattering (Table 2). The hydrodynamic radius of parent MgAl-LDH determined was ~253 nm, suggesting that only two or three LDH particles were loosely agglomerated in aqueous state. The aggregation of LDH naturally occurs under water circumstances due to the strong edge-to-face interaction [47]. As hydrothermal treatment reduces unsaturated coordination site at the edge of particle [48], agglomeration among LDHs was fairly prevented. After Ga³⁺ incorporation, hydrodynamic radius of Ga@LDH showed similar value compared with parent LDH throughout 24 h of hydrothermal treatments. Under hydrothermal process, the smooth particle edge, i.e., reduction in unsaturated coordination, would maintain to prevent serious particle aggregation. It is known that the appropriate particle size of LDH facilitates cellular uptake by target cells [8], prolongs systemic circulation [30], and enables enhanced permeation and retention (EPR) [12,49,50]; therefore, stabilized hydrodynamic radius is an advantageous point of Ga@LDHs in biomedical application.

The positive surface charge is also one of the characteristic features of LDH, and thus, time-dependent zeta potential was monitored to comprehend surface chemistry of Ga@LDHs. The zeta potential of parent LDH was around +33.8 mV (Table 2), which well

matched with the previous report [27]. The zeta potential slightly decreased at 2 h but readily recovered its positive value over +30 mV throughout 24 h (Table 2), suggesting the global surface characteristic of LDH maintained during Ga^{3+} incorporation reaction. It should be also noted that the zeta potential measurement let us exclude the formation of GaOOH impurity, which is thermodynamically stable under hydroxide-rich condition. It is reported that the GaOOH had negative zeta potential (-23 mV) in deionized water [51], which we could not find in our samples.

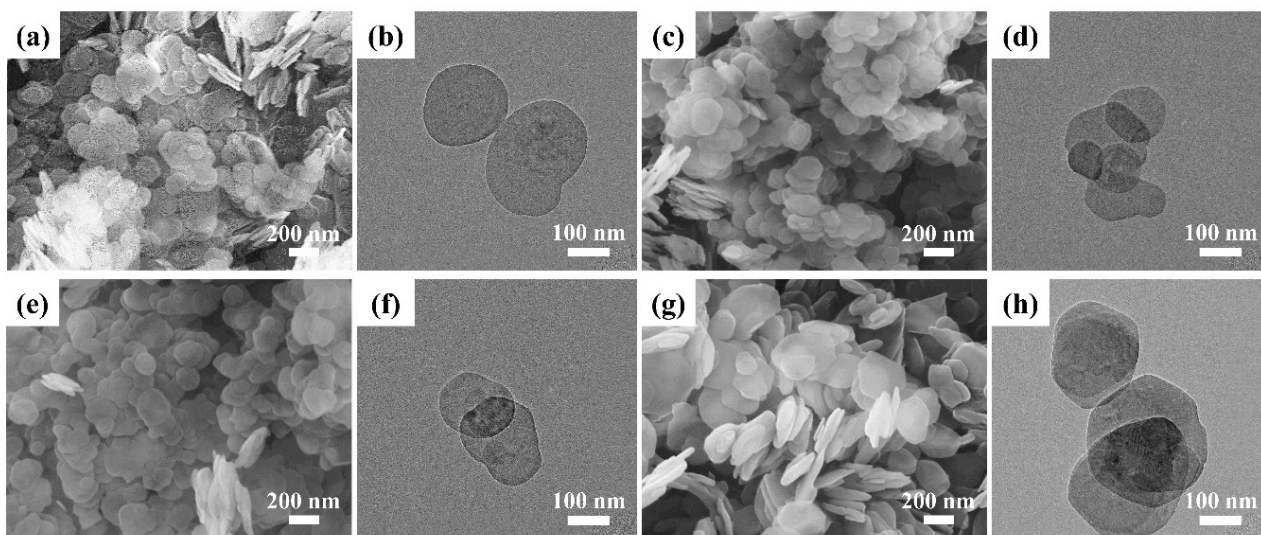


Figure 3. Scanning and transmission electron microscope image of (a,b) pristine MgAl-LDH, (c,d) Ga@LDH-0.5, (e,f) Ga@LDH-2, and (g,h) Ga@LDH-24.

Table 2. Hydrodynamic radii, zeta potential, and particle dimension of parent LDH and Ga@LDHs.

Sample	Colloidal Properties		Particle Dimension (nm) ^a	
	Hydrodynamic Radii (nm)	Zeta Potential (mV)	Lateral	Thickness
MgAl-LDH	253.5 ± 44.5	+33.8 ± 0.8	142.6 ± 35.6	18.9 ± 3.7
Ga@LDH-0.5	253.9 ± 61.2	+32.4 ± 0.5	137.5 ± 40.5	18.9 ± 3.0
Ga@LDH-1	285.7 ± 72.8	+32.9 ± 0.9	138.7 ± 38.2	21.3 ± 3.0
Ga@LDH-2	233.4 ± 35.0	+30.9 ± 0.3	139.2 ± 42.2	21.7 ± 3.3
Ga@LDH-3	256.6 ± 59.4	+32.5 ± 0.7	144.1 ± 44.0	26.1 ± 3.8
Ga@LDH-6	276.0 ± 59.3	+35.2 ± 1.6	139.2 ± 40.5	32.8 ± 5.3
Ga@LDH-12	266.3 ± 55.5	+32.4 ± 1.3	144.4 ± 49.9	36.8 ± 4.4
Ga@LDH-24	242.4 ± 39.0	+32.2 ± 0.8	146.7 ± 31.9	41.8 ± 5.9

^a Calculated as the average of 50 randomly selected particles from SEM images.

3.5. Distribution and Local Environments of Incorporated Ga^{3+} in Ga@LDH

The distribution of Ga^{3+} ion in the LDH after incorporation was visualized with scanning transmission electron microscopy (STEM)-energy dispersive spectroscopy (EDS) mapping (Figure 4 and Figure S3). To define the distribution of metal ions (Mg^{2+} , Al^{3+} , and Ga^{3+}) in LDH and Ga@LDH, EDS mapping was carried out with high-angle annular dark-field (HAADF) image containing a few particles. As shown in Figure 4, green, yellow, and magenta colors indicated the location of Mg^{2+} , Al^{3+} , and Ga^{3+} , respectively. Parent MgAl-LDH showed homogenous distribution of Mg^{2+} and Al^{3+} without development of magenta color. The incorporated Ga^{3+} was heterogeneously located in the edge of LDH particles at early time (Figure S3) as suggested in Scheme 1. After 24 h, (Figure 4B), the Ga^{3+} became homogeneously distributed throughout the LDH particle, supporting the time-dependent stabilization of LDH frameworks with balanced divalent (Mg^{2+}) and

trivalent (Al^{3+} and Ga^{3+}) cations. This observation well matched with the quantification result summarized in Table 1.

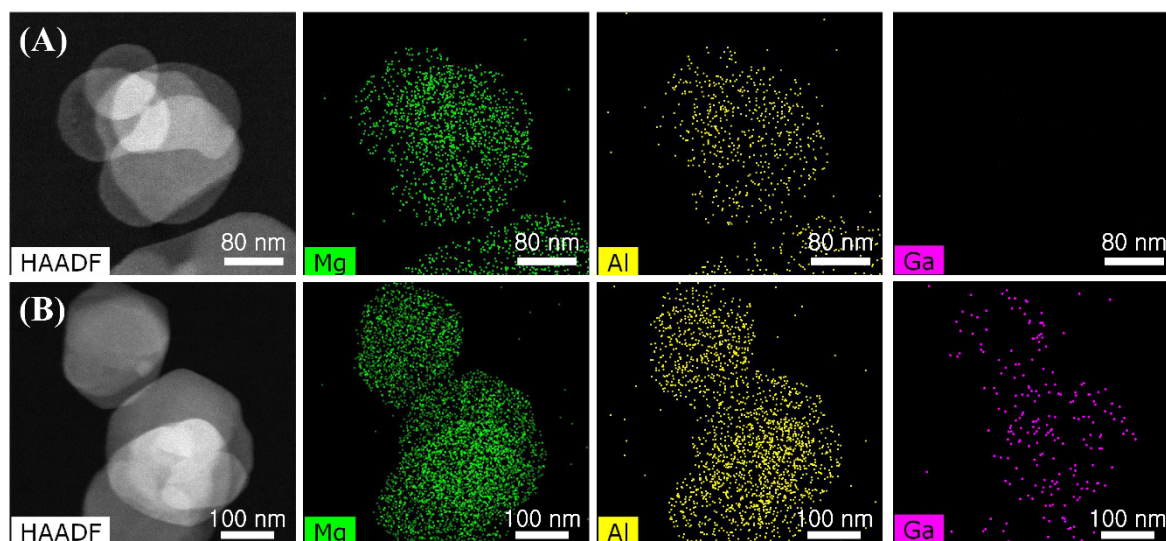


Figure 4. High-angle annular dark-field (HAADF) and element mapping images from transmission electron microscope on (A) parent MgAl-LDH and (B) Ga@LDH-24.

To determine the local chemical environment around incorporated Ga^{3+} , X-ray absorption near-edge structure (XANES) and extended X-ray absorption fine structure (EXAFS) were analyzed, as the techniques are sensitive and powerful method to investigate delicate changes in coordinate compound around a certain element. The XANES spectra of Ga@LDHs with main edge at $\sim 10,370$ eV ($1s \rightarrow 4p$ transition) [52] were fairly similar to that of MgGa-LDH—reference sample with stabilized Ga^{3+} in LDH structure—in terms of shape and sharpness, suggesting that the Ga^{3+} was well immobilized in LDH particles from 0.5 h. Slight difference in white line intensity indicated that the immobilized Ga^{3+} underwent chemical change inside the LDH particle. The white line intensity increment on Ga K-edge upon time was attributed to the strengthened Ga-O interaction through crystal rearrangement [53], in parallel with the finding in XRD analyses. At early stage of reaction, Ga^{3+} was considered to form low crystalline $\text{Ga}(\text{OH})_3$. Along the reaction time, $\text{Ga}(\text{OH})_6$ octahedron can be crystallized through homogeneous migration into LDH lattice (Scheme 1 (c)). After 24 h, Ga@LDH and reference sample, MgGa-LDH, showed almost identical white line intensity indicating that local structure around Ga^{3+} was stabilized. To precisely determine the main edge energy, first derivative of XANES spectrum was obtained (Figure 5B). It was found that the main edge energy of Ga@LDH shifted from 10,371.5 to 10,372.2 eV along the reaction time. This kind of shift was related to the increase in coordination number [54], which meant that Ga^{3+} migrated from defect site at the edge to crystalline site of center. In order to comprehend the local chemical environment around Ga^{3+} ions in Ga@LDH, R-space EXAFS spectra at Ga K-edge were analyzed (Figure 5C). It could clearly observe the first shell at 1.6 Å (nonphase-shift-corrected) and second peak at around 2.8 Å, which were attributed to the hexa-coordinate Ga-O and the neighboring metal ions such as Mg or Al [55,56]. It should be noted here that the FT amplitude of second shell is significantly lower than that of first shell (Figure 5C). According to the literatures, GaOOH [57] or Ga_2O_3 [58] showed both first and second shell peaks at similar position compared with MgGa-LDH. However, the FT amplitude of second shell in GaOOH or Ga_2O_3 was comparable with that of first shell due to the electron-rich nature of second shell Ga. The EXAFS spectra of current Ga@LDHs showed reduced peak at second shell, excluding the existence of GaOOH or Ga_2O_3 . The XANES and EXAFS spectra revealed that incorporated Ga^{3+} ions were stabilized in the LDH frameworks with same local structure of Ga-containing LDH prepared by coprecipitation method. According to the suggested

mechanism of Ga^{3+} incorporation (Scheme 1), $\text{Ga}(\text{OH})_3$ formed at early stage with low crystallinity transformed to better crystalline phase $\text{Ga}(\text{OH})_6$ upon reaction, reducing unsaturated coordination, which led to positive shift of edge energy. From the XAS results, it was found that around 0.5 h (shorter than half-life of ^{68}Ga RI) of post hydrothermal reaction was fairly enough to immobilized Ga^{3+} moiety in LDH particle, whereas crystalline rearrangement took longer time.

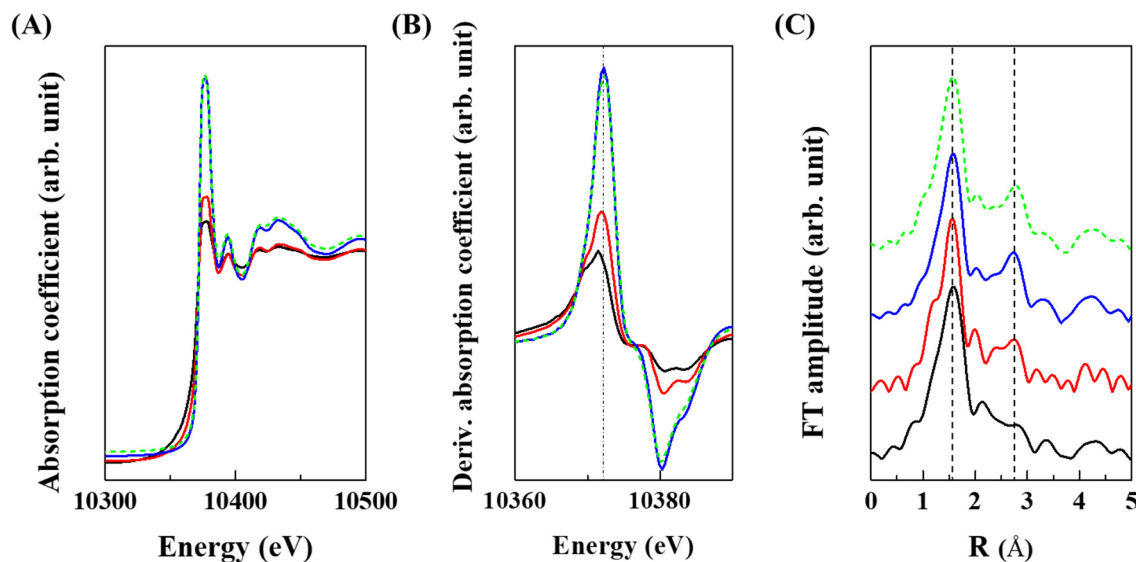


Figure 5. Ga k-edge (A) X-ray absorption near-edge structure, (B) derived X-ray absorption near-edge spectra, and (C) Fourier-transform extended X-ray absorption fine structure (FT-EXAFS) spectra of Ga@LDH-0.5 (black line), Ga@LDH-1 (red line), Ga@LDH-24 (blue line), and MgGa-LDH (green dots).

4. Conclusions

The trivalent Ga^{3+} ions were successfully incorporated into MgAl-LDH lattice via postsynthetic hydrothermal treatment. The amount of incorporated Ga^{3+} gradually increased along the reaction time with decrement of Al^{3+} fraction. From quantification of metal ions in solid product, the incorporation of Ga^{3+} was closely related to the partial dissolution of Mg^{2+} moiety at first early stage and following replacement of Al^{3+} by Ga^{3+} in solid state. The absence of thermodynamically stable gallium phase, GaOOH , suggested that the reacted Ga^{3+} was well incorporated in LDH lattice. The morphology and surface properties of LDH were maintained throughout Ga^{3+} incorporation, suggesting that this method is advantageous labeling preserving physicochemical property of parent LDH. Visualized location of incorporated Ga^{3+} by EDS mapping indicated the homogeneously distribution starting from the edge of LDH particle. From XANES and EXAFS spectra, it suggests that Ga moiety was incorporated into LDH with low crystallinity but gradually crystallized upon hydrothermal treatment. Therefore, we could conclude that the postsynthetic hydrothermal treatment of LDH with trivalent metal ion was efficient way of metal incorporation at short time, which is especially required in RI tagging in LDH.

Supplementary Materials: The following are available online at <https://www.mdpi.com/2079-4991/11/1/44/s1>, Figure S1: X-ray diffraction patterns of (a) parent MgAl-layered double hydroxide (LDH), (b–h) Ga@LDHs (0.5, 1, 2, 3, 6, 12, and 24 h); Figure S2: Scanning electron microscope image of (a) Ga@LDH-1, (b) Ga@LDH-3, (c) Ga@LDH-6, and (d) Ga@LDH-12, Figure S3: High-angle annular dark-field (HAADF) and element mapping images from scanning transmission electron microscope on (A) Ga@LDH-0.5 and (B) Ga@LDH-2 and Figure S4: Ga k-edge X-ray absorption spectroscopy spectra of Ga@LDHs (black, red, magenta, violet, orange, cyan, and blue line for 0.5, 1, 2, 3, 6, 12, and 24 h) and

MgGa-CO₃ LDH (green line). (A) X-ray absorption near-edge structure, (B) derived X-ray absorption near-edge spectra, and (C) Fourier-transform extended X-ray absorption fine structure (FT-EXAFS).

Author Contributions: Conceptualization, J.-M.O.; methodology, D.-G.J. and T.-H.K.; software, D.-G.J.; validation, D.-G.J.; formal analysis, D.-G.J. and T.-H.K.; investigation, D.-G.J.; resources, J.-M.O.; data curation, D.-G.J. and T.-H.K.; writing—original draft preparation, D.-G.J.; writing—review and editing, T.-H.K. and J.-M.O.; visualization, D.-G.J. and T.-H.K.; supervision, T.-H.K. and J.-M.O.; project administration, J.-M.O.; funding acquisition, J.-M.O. All authors have read and agreed to the published version of the manuscript.

Funding: This work was supported by the Radiation Technology R&D program and Basic Science Research Program through the National Research Foundation of Korea funded by the Ministry of Science and ICT & Future Planning (2017M2A2A6A05016600, 2017M2A2A6A05093711, and 2020R1F1A1073107) and following are results of a study on the “Leaders in INdustry-university Cooperation+” Project, supported by the Ministry of Education and National Research Foundation of Korea.

Institutional Review Board Statement: Not applicable.

Informed Consent Statement: Not applicable.

Data Availability Statement: The data presented in this study are available on request from the corresponding author.

Conflicts of Interest: The authors declare no conflict of interest. The funders had no role in the design of the study; in the collection, analyses, or interpretation of data; in the writing of the manuscript; or in the decision to publish the results.

References

1. Senapati, S.; Mahanta, A.K.; Kumar, S.; Maiti, P. Controlled drug delivery vehicles for cancer treatment and their performance. *Signal Transduct. Target. Ther.* **2018**, *3*, 1–19. [[CrossRef](#)] [[PubMed](#)]
2. Rives, V.; Del Arco, M.; Martín, C. Intercalation of drugs in layered double hydroxides and their controlled release: A review. *Appl. Clay Sci.* **2014**, *88*, 239–269. [[CrossRef](#)]
3. Cavani, F.; Trifiro, F.; Vaccari, A. Hydrotalcite-type anionic clays: Preparation, properties and applications. *Catal. Today* **1991**, *11*, 173–301. [[CrossRef](#)]
4. Khan, A.I.; O’Hare, D. Intercalation chemistry of layered double hydroxides: Recent developments and applications. *J. Mater. Chem.* **2002**, *12*, 3191–3198. [[CrossRef](#)]
5. Oh, J.-M.; Choi, S.-J.; Lee, G.-E.; Han, S.-H.; Choy, J.-H. Inorganic drug-delivery nanovehicle conjugated with cancer-cell-specific ligand. *Adv. Funct. Mater.* **2009**, *19*, 1617–1624. [[CrossRef](#)]
6. Choy, J.-H.; Choi, S.-J.; Oh, J.-M.; Park, T. Clay minerals and layered double hydroxides for novel biological applications. *Appl. Clay Sci.* **2007**, *36*, 122–132. [[CrossRef](#)]
7. Choy, J.-H.; Kwak, S.-Y.; Park, J.-S.; Jeong, Y.-J.; Portier, J. Intercalative nanohybrids of nucleoside monophosphates and DNA in layered metal hydroxide. *J. Am. Chem. Soc.* **1999**, *121*, 1399–1400. [[CrossRef](#)]
8. Oh, J.-M.; Choi, S.-J.; Lee, G.-E.; Kim, J.-E.; Choy, J.-H. Inorganic metal hydroxide nanoparticles for targeted cellular uptake through clathrin-mediated endocytosis. *Chem.-Asian J.* **2009**, *4*, 67–73. [[CrossRef](#)]
9. Kang, H.; Kim, H.-J.; Yang, J.-H.; Kim, T.-H.; Choi, G.; Paek, S.-M.; Choi, A.-J.; Choy, J.-H.; Oh, J.-M. Intracrystalline structure and release pattern of ferulic acid intercalated into layered double hydroxide through various synthesis routes. *Appl. Clay Sci.* **2015**, *112*, 32–39. [[CrossRef](#)]
10. Oh, J.-M.; Park, M.; Kim, S.-T.; Jung, J.-Y.; Kang, Y.-G.; Choy, J.-H. Efficient delivery of anticancer drug MTX through MTX-LDH nanohybrid system. *J. Phys. Chem. Solids* **2006**, *67*, 1024–1027. [[CrossRef](#)]
11. Kim, H.-J.; Lee, G.J.; Choi, A.-J.; Kim, T.-H.; Kim, T.-I.; Oh, J.-M. Layered double hydroxide nanomaterials encapsulating Angelica gigas Nakai extract for potential anticancer nanomedicine. *Front. Pharmacol.* **2018**, *9*, 723. [[CrossRef](#)] [[PubMed](#)]
12. Shi, S.; Fliss, B.C.; Gu, Z.; Zhu, Y.; Hong, H.; Valdovinos, H.F.; Hernandez, R.; Goel, S.; Luo, H.; Chen, F. Chelator-free labeling of layered double hydroxide nanoparticles for in vivo PET imaging. *Sci. Rep.* **2015**, *5*, 16930. [[CrossRef](#)] [[PubMed](#)]
13. Choy, J.-H.; Kwak, S.-Y.; Jeong, Y.-J.; Park, J.-S. Inorganic layered double hydroxides as nonviral vectors. *Angew. Chem.-Int. Edit.* **2000**, *39*, 4041–4045. [[CrossRef](#)]
14. Thurn, K.T.; Paunesku, T.; Wu, A.; Brown, E.M.; Lai, B.; Vogt, S.; Maser, J.; Aslam, M.; Dravid, V.; Bergan, R. Labeling TiO₂ nanoparticles with dyes for optical fluorescence microscopy and determination of TiO₂-DNA nanoconjugate stability. *Small* **2009**, *5*, 1318–1325. [[CrossRef](#)]
15. Kim, S.Y.; Oh, J.-M.; Lee, J.S.; Kim, T.-J.; Choy, J.-H. Gadolinium (III) diethylenetriamine pentaacetic acid/layered double hydroxide nanohybrid as novel T₁-magnetic resonant nanoparticles. *J. Nanosci. Nanotechnol.* **2008**, *8*, 5181–5184. [[CrossRef](#)]

16. Sun Zhou, X.D.; Marzke, R.; Peng, Z.; Szilágyi, I.; Dey, S.K. Understanding the High Longitudinal Relaxivity of Gd (DTPA)-Intercalated (Zn, Al)-Layered Double Hydroxide Nanoparticles. *Inorg. Chem.* **2019**, *58*, 12112–12121. [[CrossRef](#)]
17. Usman, M.S.; Hussein, M.Z.; Kura, A.U.; Fakurazi, S.; Masarudin, M.J.; Saad, F.F.A. Chlorogenic acid intercalated Gadolinium–Zinc/Aluminium layered double hydroxide and gold nanohybrid for MR imaging and drug delivery. *Mater. Chem. Phys.* **2020**, *240*, 122232. [[CrossRef](#)]
18. Li, C.; Wang, G.; Evans, D.G.; Duan, X. Incorporation of rare-earth ions in Mg–Al layered double hydroxides: Intercalation with an [Eu (EDTA)]–chelate. *J. Solid State Chem.* **2004**, *177*, 4569–4575. [[CrossRef](#)]
19. Lee, B.-I.; Lee, K.S.; Lee, J.H.; Lee, I.S.; Byeon, S.-H. Synthesis of colloidal aqueous suspensions of a layered gadolinium hydroxide: A potential MRI contrast agent. *Dalton Trans.* **2009**, 2490–2495. [[CrossRef](#)]
20. Eom, S.; Choi, G.; Choy, J.-H. Y (III) ion substituted 2D anionic clay (I); in-vitro cytotoxicity and intercellular uptake behavior. *Appl. Clay Sci.* **2019**, *176*, 58–65. [[CrossRef](#)]
21. Al Moudi, M.; Sun, Z.; Lenzo, N. Diagnostic value of SPECT, PET and PET/CT in the diagnosis of coronary artery disease: A systematic review. *Biomed. Imaging Interv. J.* **2011**, *7*. [[CrossRef](#)]
22. Sun, X.; Cai, W.; Chen, X. Positron emission tomography imaging using radiolabeled inorganic nanomaterials. *Accounts Chem. Res.* **2015**, *48*, 286–294. [[CrossRef](#)] [[PubMed](#)]
23. Xing, Y.; Zhao, J.; Conti, P.S.; Chen, K. Radiolabeled nanoparticles for multimodality tumor imaging. *Theranostics* **2014**, *4*, 290. [[CrossRef](#)] [[PubMed](#)]
24. Mizuno, Y.; Uehara, T.; Hanaoka, H.; Endo, Y.; Jen, C.-W.; Arano, Y. Purification-free method for preparing technetium-99m-labeled multivalent probes for enhanced in vivo imaging of saturable systems. *J. Med. Chem.* **2016**, *59*, 3331–3339. [[CrossRef](#)]
25. Aalbersberg, E.A.; De Wit–Van Der Veen, B.; Zwaagstra, O.; Codée–Van Der Schilden, K.; Vegt, E.; Vogel, W.V. Preclinical imaging characteristics and quantification of Platinum-195m SPECT. *Eur. J. Nucl. Med. Mol. Imaging* **2017**, *44*, 1347–1354. [[CrossRef](#)]
26. Musumeci, A.W.; Schiller, T.L.; Xu, Z.P.; Minchin, R.F.; Martin, D.J.; Smith, S.V. Synthesis and characterization of dual radiolabeled layered double hydroxide nanoparticles for use in in vitro and in vivo nanotoxicology studies. *J. Phys. Chem. C* **2010**, *114*, 734–740. [[CrossRef](#)]
27. Kim, T.-H.; Lee, J.Y.; Kim, M.-K.; Park, J.H.; Oh, J.-M. Radioisotope Co-57 incorporated layered double hydroxide nanoparticles as a cancer imaging agent. *RSC Adv.* **2016**, *6*, 48415–48419. [[CrossRef](#)]
28. Kim, H.-J.; Lee, J.Y.; Kim, T.-H.; Gwak, G.-H.; Park, J.H.; Oh, J.-M. Radioisotope and anticancer agent incorporated layered double hydroxide for tumor targeting theranostic nanomedicine. *Appl. Clay Sci.* **2020**, *186*, 105454. [[CrossRef](#)]
29. Oh, J.-M.; Choi, S.-J.; Kim, S.-T.; Choy, J.-H. Cellular uptake mechanism of an inorganic nanovehicle and its drug conjugates: Enhanced efficacy due to clathrin-mediated endocytosis. *Bioconjug. Chem.* **2006**, *17*, 1411–1417. [[CrossRef](#)]
30. Choi, S.-J.; Oh, J.-M.; Choy, J.-H. Biocompatible nanoparticles intercalated with anticancer drug for target delivery: Pharmacokinetic and biodistribution study. *J. Nanosci. Nanotechnol.* **2010**, *10*, 2913–2916. [[CrossRef](#)]
31. Lundehøj, L.; Cellier, J.; Forano, C.; Nielsen, U.G. Atomic Level Understanding of Orthophosphate Adsorption by Magnesium Aluminum-Layered Double Hydroxides—A Multitechnique Study. *J. Phys. Chem. C* **2019**, *123*, 24039–24050. [[CrossRef](#)]
32. Unal, U. Short-time hydrothermal synthesis and delamination of ion exchangeable Mg/Ga layered double hydroxides. *J. Solid State Chem.* **2007**, *180*, 2525–2533. [[CrossRef](#)]
33. Oh, J.-M.; Hwang, S.-H.; Choy, J.-H. The effect of synthetic conditions on tailoring the size of hydrotalcite particles. *Solid State Ion.* **2002**, *151*, 285–291. [[CrossRef](#)]
34. Xu, Z.P.; Stevenson, G.; Lu, C.Q.; Lu, G.Q. Dispersion and size control of layered double hydroxide nanoparticles in aqueous solutions. *J. Phys. Chem. B* **2006**, *110*, 16923–16929. [[CrossRef](#)]
35. Choi, G.; Kwon, O.-J.; Oh, Y.; Yun, C.-O.; Choy, J.-H. Inorganic nanovehicle targets tumor in an orthotopic breast cancer model. *Sci. Rep.* **2014**, *4*, 1–7. [[CrossRef](#)]
36. Kumar, V.; Boddeti, D.K. 68 Ga-radiopharmaceuticals for PET imaging of infection and inflammation. In *Theranostics, Gallium-68, and Other Radionuclides*; Springer: Berlin/Heidelberg, Germany, 2013; pp. 189–219. [[CrossRef](#)]
37. Müller, C.; Bunka, M.; Reber, J.; Fischer, C.; Zhernosekov, K.; Türler, A.; Schibli, R. Promises of cyclotron-produced 44Sc as a diagnostic match for trivalent β^- -emitters: In vitro and in vivo study of a 44Sc-DOTA-folate conjugate. *J. Nucl. Med.* **2013**, *54*, 2168–2174. [[CrossRef](#)]
38. Kim, T.-H.; Lee, W.-J.; Lee, J.-Y.; Paek, S.-M.; Oh, J.-M. Isomorphous substitution of divalent metal ions in layered double hydroxides through a soft chemical hydrothermal reaction. *Dalton Trans.* **2014**, *43*, 10430–10437. [[CrossRef](#)]
39. Shin, J.; Choi, C.-J.; Kim, T.-H.; Oh, J.-M. Phase Transformation from Brucite to Highly Crystalline Layered Double Hydroxide through a Combined Dissolution–Reprecipitation and Substitution Mechanism. *Cryst. Growth Des.* **2018**, *18*, 5398–5405. [[CrossRef](#)]
40. Cullity, B. *Elements of X-ray Diffraction*; Addison-Wesley Publishers: Boston, MA, USA, 1978.
41. Palin, L.; Milanesio, M.; Van Beek, W.; Conterposito, E. Understanding the ion exchange process in LDH nanomaterials by fast in situ XRPD and PCA-assisted kinetic analysis. *J. Nanomater.* **2019**, *2019*, 4612493. [[CrossRef](#)]
42. Komarneni, S.; Kozai, N.; Roy, R. Novel function for anionic clays: Selective transition metal cation uptake by diadochy. *J. Mater. Chem.* **1998**, *8*, 1329–1331. [[CrossRef](#)]
43. Rives, V. *Layered Double Hydroxides: Present and Future*; Nova Publishers: Hauppauge, NY, USA, 2001.
44. Ogawa, M.; Asai, S. Hydrothermal synthesis of layered double hydroxide– deoxycholate intercalation compounds. *Chem. Mater.* **2000**, *12*, 3253–3255. [[CrossRef](#)]

45. Wijitwongwan, R.P.; Intasa-ard, S.G.; Ogawa, M. Preparation of Layered Double Hydroxides toward Precisely Designed Hierarchical Organization. *ChemEngineering* **2019**, *3*, 68. [[CrossRef](#)]
46. Liu, H.; Wang, Y.; Lu, X.; Hu, Y.; Zhu, G.; Chen, R.; Ma, L.; Zhu, H.; Tie, Z.; Liu, J. The effects of Al substitution and partial dissolution on ultrathin NiFeAl ternary layered double hydroxide nanosheets for oxygen evolution reaction in alkaline solution. *Nano Energy* **2017**, *35*, 350–357. [[CrossRef](#)]
47. Clark, I.; Gomes, R.L.; Crawshaw, C.; Neve, L.; Lodge, R.; Fay, M.; Winkler, C.; Hull, M.; Lester, E. Continuous synthesis of Zn₂Al–CO₃ layered double hydroxides: A comparison of bench, pilot and industrial scale syntheses. *React. Chem. Eng.* **2019**, *4*, 663–666. [[CrossRef](#)]
48. Choi, G.; Piao, H.; Alothman, Z.A.; Vinu, A.; Yun, C.-O.; Choy, J.-H. Anionic clay as the drug delivery vehicle: Tumor targeting function of layered double hydroxide-methotrexate nanohybrid in C33A orthotopic cervical cancer model. *Int. J. Nanomed.* **2016**, *11*, 337. [[CrossRef](#)]
49. Choi, G.; Kim, S.Y.; Oh, J.-M.; Choy, J.-H. Drug-Ceramic 2-Dimensional Nanoassemblies for Drug Delivery System in Physiological Condition. *J. Am. Ceram. Soc.* **2012**, *95*, 2758–2765. [[CrossRef](#)]
50. Wang, L.; Huang, J.; Chen, H.; Wu, H.; Xu, Y.; Li, Y.; Yi, H.; Wang, Y.A.; Yang, L.; Mao, H. Exerting enhanced permeability and retention effect driven delivery by ultrafine iron oxide nanoparticles with T 1–T 2 switchable magnetic resonance imaging contrast. *ACS Nano* **2017**, *11*, 4582–4592. [[CrossRef](#)]
51. Huang, C.-C.; Yeh, C.-S.; Ho, C.-J. Laser ablation synthesis of spindle-like gallium oxide hydroxide nanoparticles with the presence of cationic cetyltrimethylammonium bromide. *J. Phys. Chem. B* **2004**, *108*, 4940–4945. [[CrossRef](#)]
52. Pickup, D.M.; Valappil, S.P.; Moss, R.M.; Twyman, H.; Guerry, P.; Smith, M.E.; Wilson, M.; Knowles, J.C.; Newport, R.J. Preparation, structural characterisation and antibacterial properties of Ga-doped sol–gel phosphate-based glass. *J. Mater. Sci.* **2009**, *44*, 1858–1867. [[CrossRef](#)]
53. Chao, K.-J.; Wei, A.C. Characterization of heterogeneous catalysts by X-ray absorption spectroscopy. *J. Electron Spectrosc. Relat. Phenom.* **2001**, *119*, 175–184. [[CrossRef](#)]
54. Nishi, K.; Shimizu, K.-I.; Takamatsu, M.; Yoshida, H.; Satsuma, A.; Tanaka, T.; Yoshida, S.; Hattori, T. Deconvolution analysis of Ga K-Edge XANES for quantification of gallium coordinations in oxide environments. *J. Phys. Chem. B* **1998**, *102*, 10190–10195. [[CrossRef](#)]
55. Basu, S.; Naidu, B.S.; Pandey, M.; Sudarsan, V.; Jha, S.N.; Bhattacharyya, D.; Vatsa, R.K.; Kshirsagar, R.J. Eu³⁺ assisted structural collapse of GaOOH nanorods: Probed through EXAFS and vibrational techniques. *Chem. Phys. Lett.* **2012**, *528*, 21–25. [[CrossRef](#)]
56. Defontaine, G.; Michot, L.J.; Bihannic, I.; Ghanbaja, J.; Briois, V. Synthesis of NiGa layered double hydroxides. A combined EXAFS, SAXS, and TEM study. 3. Synthesis at constant pH. *Langmuir* **2004**, *20*, 11213–11222. [[CrossRef](#)] [[PubMed](#)]
57. Pokrovski, G.S.; Schott, J.; Hazemann, J.L.; Farges, F.; Pokrovsky, O.S. An X-ray absorption fine structure and nuclear magnetic resonance spectroscopy study of gallium–silica complexes in aqueous solution. *Geochim. Cosmochim. Acta* **2002**, *66*, 4203–4222. [[CrossRef](#)]
58. Sharma, A.; Varshney, M.; Shin, H.J.; Chae, K.H.; Won, S.O. Investigation on cation distribution and luminescence in spinel phase γ -Ga_{3– δ O₄: Sm nanostructures using X-ray absorption spectroscopy. *RSC Adv.* **2017**, *7*, 52543–52554. [[CrossRef](#)]}